Title
MASS TRANSFER ENHANCEMENT BY SMALL FLOW OBSTACLES IN ELECTROCHEMICAL CELLS

Author
Fischl, D.S.

Publication Date
1984-11-01

Lawrence Berkeley Laboratory
UNIVERSITY OF CALIFORNIA

Materials & Molecular Research Division

Submitted to Chemical Engineering Communications

MASS TRANSFER ENHANCEMENT BY SMALL FLOW OBSTACLES IN ELECTROCHEMICAL CELLS

D.S. Fischl, K.J. Hanson, R.H. Muller, and C.W. Tobias

November 1984

Prepared for the U.S. Department of Energy under Contract DE-AC03-76SF00098

DISCLAIMER

MASS TRANSFER ENHANCEMENT BY SMALL FLOW OBSTACLES IN ELECTROCHEMICAL CELLS

D.S. FISCHL, K.J. HANSON, R.H. MULLER & C.W. TOBIAS

Materials and Molecular Research Division
Lawrence Berkeley Laboratory
and Department of Chemical Engineering
University of California
Berkeley, CA 94720

ABSTRACT

Mass transfer enhancement by small obstacles attached to the cathode in electrolytic flow cells of 5 x 5 mm cross-section and 500 mm length was investigated. Double beam laser interferometry was used to observe the local mass transfer boundary layer thicknesses preceding and following rod- shaped dielectric obstacles placed normal to the direction of electrolyte flow. Flow patterns have been visualized by use of suspensions of small inert particles and dark field photography. For the evaluation of the effectiveness of mass transport enhancement, pressure drops, and limiting currents for the reduction of ferricyanide have been measured in the range of Reynolds Number 80 to 3200. The degree of enhancement increases with decreasing obstacle spacing until an optimal spacing of approximately 15 times the obstacle size is reached. A three to five- fold increase in the average mass transfer coefficient is achieved by the use of obstacles with a small fraction of the pumping power required to obtain the same limiting current by increasing the flow rate in the unobstructed channel. Small obstacles produce efficient mixing near the electrode surface, and corresponding improvement in uniformity and magnitude of mass transport rates, without increasing the energy dissipation in the bulk fluid.

1. INTRODUCTION

When the rate of an electrode process is restricted by mass transfer to the electrode surface, flow obstacles can enhance the rate of convective diffusion at a fraction of the pumping demand required if the flow rate were to be increased instead. In applications such as electrodialysis, ultra-filtration, and reverse osmosis, substantial increases in limiting current relative to the smooth channel has been demonstrated (Solan et al., 1971; Leitz and Marincic, 1977; Storck and Hutin, 1981).

Previous investigations of flow obstacles have largely been focused on systems in which the obstacles were large relative to the interelectrode gap. Such obstacles had the effect of producing fully turbulent flow at relatively low volumetric flow rates. For example, Solan, et al. (1971), used large plastic spacer nets which acted as turbulence promoters at low flow rates. Other types of turbulence promoters were investigated by Leitz and Marincic, (1977), Sonin and Isaacson (1974), Storck et al. (1978, 1981), Shen and Probstein (1979), Kang and Chang (1982), and Focke (1983). Schalch and Ibl (1975) presented a technique for increasing mass transfer in a stagnant bath-type electrochemical cell by wiping the electrode surface with moving nets. The use of finely woven stationary nets or cloths to increase mass transfer rates was subsequently extended by Robertson, et al. (1975) and employed in the design of the "Swiss Roll Cell" (Robertson and Ibl, 1977; Schwager, et al. 1980). An industrial application of the "Swiss Roll Cell" has recently been reported (Robertson et al., 1983).

In contrast to previous work we report here on investigations in which the diameter of rods placed in a laminar flow field was chosen to be small

relative to the channel dimensions (10-15% of inter-electrode gap), with large spacings between the obstacles.

Two techniques were used to study the effect of flow obstacles: To evaluate local changes in the boundary layer thickness near the obstacle, interferometry experiments were performed. This initial study was designed to determine the effect of the size, shape and location of the obstacle on the local concentration profile. Subsequently, the cumulative effect of regularly spaced obstacles was evaluated by measuring the average limiting current for the reduction of ferri- to ferro- cyanide as it depends on the number and size of the obstacles. Pressure drop measurements were performed to determine the optimal spacing of obstacles for maximum enhancement of mass transfer with a minimum increase in pressure drop.

2. INTERFEROMETRIC STUDY

a. Apparatus

A parallel- plate electrochemical flow cell was built to perform interferometric measurements of the mass transfer boundary layer as a function of the distance from the leading edge of the electrode and also near flow obstacles. Deposition of copper from an unsupported copper sulfate electrolyte (0.05 M) was used as a model reaction. The cell, shown in Fig. 1, was constructed of acrylic resin with parallel, optically flat glass walls. Copper electrodes (99.999%) were 550 mm long and 5 mm wide and located downstream following a 60 cm long entry section, to assure a fully developed velocity profile at the electrodes. The cross-section of the channel was 5 mm square.

Both the sides and working surface of the copper electrodes were polished to a mirror finish to facilitate the alignment of the laser beam. Special techniques for polishing the electrode surface were used to minimize optical errors caused by reflection from a rounded electrode edge (McLarnon et al., 1975). Electrolyte was supplied to the cell by gravity feed. During electrolysis, the cathode was oriented face down to avoid natural convection effects. Flow obstacles were machined with triangular, square and round cross-sections from epoxy resin. Each obstacle was 0.76 mm high and extended across the entire (5 mm) width of the flow channel, the cross-section of which is schematically shown in Fig. 2.

Details of the design and use of the Mach-Zehnder interferometer employed in this investigation (Fig. 2) have already been published (Beach et al., 1969, McLarnon et al., 1976, 1979). The interference fringe patterns are related to the concentration profiles of species in the cell (Muller, 1973, 1977). Straight interference fringes, representing a homogeneous concentration field, are generated by proper alignment of the instrument. Upon passage of current, these fringes are displaced as a consequence of local refractive index changes in the boundary layer. With a knowledge of the dependence of the index of refraction on concentration, one can derive the concentration profile and boundary layer thickness from the fringe pattern (McLarnon et al., 1975 II, 1975 III, Beach et al. 1973). The fringes are recorded by a 16 mm movie camera located on the interferometer support. The optical system is mounted on a lathe bed to permit the entire electrode length to be scanned. Experimental procedures have been described in detail (Hanson, 1979).

b. Results and Discussion: Interferometry

To evaluate the effectiveness of the obstacles in disturbing the boundary layer, raw data in the form of photographs of interference fringes were reduced to plots of boundary layer thickness as a function of distance from the leading edge of the electrode. The validity of this approach was checked by measuring the boundary layer thickness in an unobstructed channel and comparing the result to the value predicted by the Leveque solution for flow between two flat plates (McLarnon et al., 1979). The experimentally- determined boundary layer thickness was in satisfactory agreement with the theoretical prediction. A typical set of interferograms, showing a square obstacle attached to the electrode surface, is given in Fig. 3. Thinning of the mass transfer boundary layer downstream from the obstacle can be clearly seen. The undisturbed profile (a) is disrupted by the obstacle located 150 mm from the leading edge of the electrode; an upstream effect of the obstacle can also be detected. In the near downstream region (b), (c), the boundary layer is narrow and local turbulence causes waviness in the appearance of the fringes in the bulk solution. As the distance from the obstacle increases, the disturbance subsides and the concentration profile appears similar to the undisturbed profile (d). An example of reduced data is given in Fig. 4, showing the ninety-nine percent boundary layer thickness as a function of the distance from an attached triangular obstacle. Note that at this Reynolds number (756), the boundary layer does not "recover" to its thickness immediately upstream of the obstacle for a downstream distance that is more than 300 times the diameter of the obstacle.

The effect of shape and position of the obstacles was evaluated by

comparing the boundary layers in the turbulent wake for each case. In each set of experiments an obstacle of different geometry, but identical height (0.76 mm), was attached to the electrode 150 mm from the leading edge. The effect of obstacle shape is shown in Fig. 5. All of the attached obstacles decrease the boundary layer thickness similarly, but the "recovery" of the boundary layer downstream of the obstacle depends upon the shape of the obstacle. As the obstacle becomes more streamlined, the boundary layer thickness reaches the upstream value over a shorter distance. Thus, the triangular shape is more effective than the square, and the square shape is more effective than the round obstacle. The boundary layer thickness in an unobstructed flow cell is also shown in Figs. 5 and 6 for comparison. Detached obstacles were tested at distances of 1, 2, and 3 obstacle diameters from the electrode surface. The effect of the distance of the obstacle from the electrode surface is shown in Fig. 6 in comparison to Fig. 5. The reduction of boundary layer thickness was found to decline as the distance from the surface was increased. The obstacle located 0.76 mm (one obstacle height) from the surface had almost the same effect on the boundary layer as an attached obstacle, while the one located in the center of the cell resulted in an undetectable change of the boundary layer thickness.

At higher flow velocity the obstacles have an effect over a greater distance. However, because the unobstructed boundary layer is also thinner at higher flow rates, the relative enhancement decreases with increasing flow rate.

3. LIMITING CURRENT AND PRESSURE DROP STUDY

a. Principles

To evaluate the cumulative effect of regularly-spaced obstacles on the average mass transfer coefficient, the limiting current technique was employed (Selman and Tobias, 1975). The pressure drop across the channel was also measured to determine pumping power requirements and, thus, the effectiveness of the mass transfer enhancement. At the limiting current density i_L (A/cm^2) the surface concentration of the reacting species is zero and the current is directly proportional to the mass transfer coefficient k (cm/sec) or the dimensionless Sherwood number Sh,

$$Sh = \frac{d_e\, i_L}{D_i\, C_b\, nF} = \frac{k\, d_e}{D_i} \qquad (1)$$

Here, D_i is the diffusion coefficient (cm^2/sec) of the reacting ion, C_b is the bulk concentration of the reacting ion ($mole/cm^3$), d_e is the equivalent hydraulic diameter (cm), n is the number of electrons transferred per reacting ion and F is Faraday's constant (96487 coul/equiv).

For channel flow the dimensionless Fanning friction factor f (Bird et al., 1960) is given by:

$$f = \frac{1}{4}\left[\frac{d_e\ \Delta P}{\frac{1}{2}\rho V_b^2\ L}\right] \qquad (2)$$

where ΔP is the pressure drop (Newtons/m^2), the fluid density, V_b the average fluid velocity and L the electrode length. The power required to pump the fluid through the channel is a product of the pressure drop and the volumetric flow rate. The pumping power requirement per unit area of the cathode, designated as specific power P_{sp} (Watt/m^2) is:

$$P_{sp} = \frac{\Delta P \cdot Q}{L \cdot W} \qquad (3)$$

where Q is the volumetric flow rate (m^3/sec), and W the electrode width.

b. Apparatus and Experiment

The flow cell used in the interferometric studies was modified for limiting current and pressure drop measurements. The copper electrodes used in the interferometric study were replaced by two nickel electrodes of 5mm width and 508 mm active length and the glass windows were replaced by acrylic sidewalls. The electrolyte used in the limiting current measurement was 0.01 M $K_3Fe(CN)_6$ and 0.05 M $K_4Fe(CN)_6$ in a 0.30 M NaOH supporting electrolyte solution. Limiting currents were determined for the cathodic reduction of the ferricyanide ion on the upper electrode. Oxidation of the ferrous to the ferric state occurred at the lower electrode. The diffusivity D_i of the reacting

ferricyanide ion $Fe(CN)_6^{3-}$ was calculated using the correlation equation by Gordon et al. (1966). Since the redox reaction does not involve a deposition process, the electrode surface remains unchanged during the measurements.

The pressure drop was measured between two pressure taps of 0.074 cm diameter, machined into the acrylic resin side wall of the cell halfway between the electrodes at the leading and trailing edges of the electrodes, 508 mm apart (Fig. 1). A diaphragm type pressure transducer (Validyne DP103) was used to monitor the pressure difference between these two sampling points.

In both the limiting current and pressure drop experiments only rectangular flow obstacles, made of acrylic resin, were used. These obstacles measured 0.76 x 0.76 x 5 mm and were attached directly to the cathode. Details of the experimental procedure have been reported elsewhere (Fischl, 1983).

c. Results and Discussion of Limiting Current and Pressure Drop Measurements

The mass transfer rate to the entire electrode was obtained by measuring the limiting current achieved in response to a potential step. The current response to the potential step is shown in Fig. 7 for different flow rates. After an initial transient, the limiting current is constant and increases with increasing Reynolds number Re. Reproducibility is within 1 percent. The onset of bulk turbulence (Re = 2170) produces sharp fluctuations in the current, as can be seen in Fig. 7.

The flow obstacles were attached directly to the cathode surface. As in the interferometric study, the ratio of the obstacle height to the electrode separation was 0.15. The total number of obstacles used in an experiment ranged from 3-49. For a given experiment the obstacles were evenly spaced along the entire electrode length with no obstacle attached to the leading or

trailing edge of the electrode. Experimental conditions are summarized in Table I. The results are presented using the number of obstacles as a parameter.

Figure 8 is a plot of the total limiting current passed to the electrode as a function of Reynolds number (based on unobstructed d_e and V_b) and number of obstacles. The dramatic increase due to the presence of obstacles is apparent. It is also quite clearly shown that although increasing the frequency of obstacles improves the average mass transfer rate to the electrode surface, once the rods are placed relatively close together, further crowding brings about no beneficial effect. As can be seen in Fig. 8, using 49 evenly-spaced rods, rather than only 31, produces no improvement in mass transfer rates.

A full characterization of size and shape effects has not been undertaken in this investigation. The main body of experimental work employed rods of 0.76 x 0.76 mm cross-section; these were the smallest sharp- edged acrylic prisms that we were able to cut readily. However, limiting currents were also obtained in an exploratory set of measurements with various placements of either larger (1.6 x 1.6 mm) or smaller (0.25 mm high x 0.76 mm wide) rods. These sizes correspond to approximately one-third and one-twentieth area occupancy of the 5 x 5 mm channel cross-section, respectively. The pressure drop, as expected, was found to increase with the larger rod without a proportionate increase in transport enhancement. Conversely, using the smaller rod, the pressure drop diminished with a more than proportionate decrease in transport enhancement. Optimal spacing of obstacles increases with increasing height; with the 1.6 mm high rods the greatest enhancement was observed with a spacing of approximately fifteen times rod height.

The dependence of the experimentally- obtained Sherwood number Sh on the

Reynolds number (Re), the Schmidt number (Sc) and the equivalent duct diameter d_e divided by the electrode length L is shown in Fig. 9. Also shown is the correlation for the laminar flow regime in unobstructed ducts of this study.

$$Sh = 1.85\Phi\left[ReSc\,\frac{d_e}{L}\right]^{1/3} \qquad (4)$$

where the correction factor $\Phi = 0.842$ for a square channel (Rousar et al., 1971).

In the laminar regime the agreement with the experimental results (solid dots) is good. More obstacles (closer spacing) produces greater mass transfer enhancement until a maximum is reached with 31 obstacles. When comparing the enhanced mass transfer rates to the rates in the unobstructed channel, the enhancement increases with increasing flow rate, until the Reynolds number exceeds 2100. At higher flow rates, bulk turbulence occurs in the duct and the relative enhancement by the obstacles is decreased. Maximum enhancement is observed just before bulk turbulence is produced in the unobstructed channel.

Figure 10 is a plot of the pressure drop as a function of flow rate and number of obstacles. The unobstructed results are compared to the exact solution for flow in a square duct given by (Purday, 1949; White, 1974):

$$\Delta P = \left[\frac{28.55\ \mu L}{d_e^2}\right] V_b \qquad (5)$$

At lower flow rates the addition of the small obstacles does not significantly increase the pressure drop. However, at higher flow rates exponential behavior is observed. The pressure drop is drastically increased by the addition of 49 obstacles. This effect, and the lack of increase in mass

transfer enhancement caused by the close spacing of obstacles (Figs. 8 and 9), leads to the conclusion that an optimum spacing exists. In this study the 31 obstacle arrangement produced the most beneficial mass transfer enhancement.

It is seen that at Re $\approx$ 100, the mass transfer rate is approximately doubled upon the addition of 31 obstacles without appreciably affecting the pressure drop. A four-fold enhancement occurs in the upper laminar flow regime with only a 3.5 fold increase in the pressure drop.

The dependence of the Fanning friction factor f on the Reynolds number Re is shown in Fig. 11. By combining Eqs (2) and (5), for laminar flow in an unobstructed square duct $f = 14.2(Re)^{-1}$. This line is presented for comparison. As the flow changes from laminar to turbulent the dependence of friction factor on Reynolds number changes from Re^{-1} to $Re^{-1/4}$ and at high Re, for hydrodynamically rough channels, the exponent approaches zero.

4. FLOW VISUALIZATION

It is evident that the addition of obstacles enhances mass transfer by changing the flow pattern near the mass-transfer surface. The flow pattern was observed and photographed using a dark field technique (Ibl and Muller, 1955). In Fig. 12 a recirculation zone is shown downstream from the obstacle. The length of this recirculation zone increases with increasing flow rate; it is also related to the obstacle height, with larger obstacles producing disturbances over a greater length.

Further visualization experiments were performed to observe the effect of obstacle spacing. With 31 obstacles, the recirculation zone reached almost to the next downstream obstacle; with 49 obstacles (attached to the electrode),

the recirculation zone extended over the entire inter-obstacle distance. Before bulk turbulence was observed in all the arrangements, the flow in the bulk was essentially laminar, while close to the wall behind the obstacle intensive mixing was produced in the swirling recirculation zone (Fig. 13). These results are consistent with the results of Focke (1983), who observed that the maximum elongation of the recirculation zone in the laminar regime is 15 times the obstacle height.

The effect of multiple obstacles on the boundary layer was also observed by the interferometric technique. Figure 14 shows the boundary layer thickness with four obstacles, obtained from interferograms. Multiple obstacles produce an average overall decrease in the boundary layer thickness which is related to the effect observed for an individual obstacle. They eliminate the continuous increase in boundary layer thickness in the downstream direction with laminar flow in the bulk fluid and, thus, result in a more uniform current distribution.

5. DISCUSSION

In comparing results obtained by the interferometric and the limiting current techniques, it is important to note the differences between the two techniques. Observation of the local boundary layer thickness by interferometry was achieved during copper deposition below the limiting current and without supporting electrolyte. In contrast, average mass transfer rates were measured for a redox reaction at limiting current in the presence of excess supporting electrolyte.

The limiting current measurements were used to calculate an effective

average boundary layer thickness δ_{99} over the entire electrode by the following relation (McLarnon, 1974):

$$\delta_{99} = \frac{2d_e}{Sh} \qquad (6)$$

The Sherwood number was obtained from Fig. 9 for the operating conditions of the interferometric study.

The profile of the boundary layer thickness over the entire (50.8 cm) electrode produced by multiple obstacles was estimated by extending the multiple obstacle effect shown in Fig. 14. An average value over the entire electrode length was then calculated. The results are summarized in Table II. The agreement is remarkably good considering the substantial differences between the techniques and the errors involved in the optical measurements (Hanson, 1979; McLarnon, 1974).

An analysis of benefits derived from the use of small flow obstacles has to be based on the specific pumping power, P_{sp}, rather than the pressure drop, ΔP. Figure 15 shows the experimental results for unobstructed and multiple obstacle cases.

The unobstructed channel requires a large input of pumping power when higher currents (mass transfer rates) must be achieved. For the unobstructed channel the flow velocity, V_b, must be greatly increased to obtain these higher currents. These large increases in the required pumping power for the unobstructed channel are produced because the bulk turbulent flow regime must be reached in order to obtain total currents over approximately 18 mA (shown in Fig. 8) corresponding to mass transfer coefficients larger than 0.8×10^{-3} cm. sec^{-1}.

In Fig. 15 the advantage of the use of 31 obstacles is clearly demonstrated.

The required pumping power is greatly reduced compared to operation at the same current (transfer rate) with the unobstructed channel. To obtain a mass transfer coefficient of $k = 1.0 \times 10^{-3}$ cm sec $^{-1}$ (25 mA current), the use of 31 attached obstacles results in a 25-fold reduction in pumping power requirement compared to achieving the same rate of mass transfer in an unobstructed channel with an increased flow rate; for $k = 1.5 \times 10^{-3}$ cm sec^{-1} (37.5 mA) a 35-fold reduction is obtained.

6. CONCLUSIONS

Attached small obstacles have been shown to increase the rate of mass transfer to the walls of a flow channel. Favorable shape, size and spacing have been identified by use of interferometric observations, flow visualization, and pressure drop and limiting current measurements. Reducing the spacing between the obstacles produces increased mass transfer enhancement; however, when the spacing is too close, effectiveness is decreased. For the rectangular obstacles the optimum spacing is approximately 15 times the obstacle height and corresponds to the maximum elongation of the downstream recirculation zone. Compared to the unobstructed channel, the obstacles provide more uniform mass transfer and a considerable reduction in the pumping power required to achieve a given average rate of mass transfer. The advantage of the flow obstacles is greatly reduced in bulk turbulent flow because their benefit derives from efficient mixing close to the wall which produces mass transfer enhancement under laminar flow in the bulk fluid.

ACKNOWLEDGMENT

This work was supported by the Director, Office of Energy Research, Office of Basic Energy Sciences, Materials Sciences Division of the U.S. Department of Energy under Contract Number DE-AC03-76SF00098

REFERENCES

Beach, K.W., R.H. Muller and C.W. Tobias, Rev. Sci. Instrum. 40, 1248 (1969).

Beach, K.W., R.H. Muller and C.W. Tobias, J. Opt. Soc. Amer. 63, 559 (1973).

Bird, R.B., W.E. Stewart and E.N. Lightfoot, Transport Phenomena; Wiley, NY (1960).

Fischl, D.S., M.S. Thesis, Dept. of Chem. Engr., University of California Berkeley, August 1983. (LBL-16422).

Focke, W.W., Electrochim. Acta 28, 1137 (1983).

Gordon, S.L., J.S. Newman and C.W. Tobias, Ber. Bunsenges. Phys. Chem. 70, 414 (1966).

Hanson, K.J., M.S. Thesis, Dept. of Chem. Eng., University of California Berkeley, April 1979. (LBL-9038).

Ibl, N. and R.H. Muller, Z. Elektrochem. Ber. Bunsenges. phys. Chem. 59, 671 (1955).

Kang, I.S. and H.N. Chang, Int. J. Heat Mass Trans. 25, 1167 (1982).

Leitz, F.B. and L. Marincic, J. Appl. Electrochem., 7, 473 (1977).

McLarnon, F.R., R.H. Muller and C.W. Tobias, Appl. Opt. 14, 2468 (1975).

McLarnon, F.R., R.H. Muller and C.W. Tobias, J. Opt. Soc. Am. 65, 1011 (1975), II.

McLarnon, F.R., R.H. Muller and C.W. Tobias, J. Electrochem. Soc. 122, 59 (1975), III.

McLarnon, F.R., R.H. Muller and C.W. Tobias, Electrochim. Acta 21, 101 (1976).

McLarnon, F.R., R.H. Muller and C.W. Tobias, Ind. Eng. Chem. Fund. 18, 97 (1979).

Muller, R. H., in Advances in Electrochemistry and Electrochemical Engineering, Vol.9,. P. Delahay and C. W. Tobias, eds., Wiley-Intersciences, New York, 1973

Muller, R.H., Electrochim. Acta 22, 951 (1977).

Purday, H.F.P., Streamline Flow, Constable, London (1949) p. 14.

Robertson, P.M., F. Schwager and N. Ibl, J. Electroanal. Chem. 65, 883 (1975).

Robertson, P.M. and N. Ibl, J. Appl. Electrochem. 7, 323 (1977).

Robertson, P.M., P. Berg, H. Reimann, K. Schleich and P. Seiler, J. Electrochem. Soc. 130, 591 (1983).

Rousar, I., J. Hostomsky and V. Cezner, J. Electrochem. Soc. 118, 881 (1971).

Schalch, E. and N. Ibl, Electrochim. Acta 20, 435 (1975).

Schwager, F., P.M. Robertson and N. Ibl, Electrochim. Acta 25, 1655 (1980).

Selman, J.R. and C.W. Tobias, J. Electroanal. Chem. 65, 67 (1975).

Shen, J.J.S. and R.F. Probstein, Ind. Eng. Chem. Proc. Des. Dev. 18, 547 (1979).

Solan, A., Y. Winograd and U. Katz, Desalination 9, 89 (1971).

Sonin, A.A. and M.S. Isaacson, Ind. Eng. Chem. Proc. Des. Dev. 13, 241 (1974).

Storck, A. and F. Coeuret, Ind. Eng. Chem. Proc. Des. Dev. 17, 99 (1978).

Storck, A. and D. Hutin, Electrochim. Acta 26, 117, 127 (1981).

Winograd, Y., A. Solan and M. Toren, Desalination 13, 171 (1973).

White, F.M., Viscous Fluid Flow, McGraw-Hill, NY (1974) p. 123.

Table I. Channel Geometry with 0.76 mm High Obstacles.

Number of Obstacles	Ratio of Obstacle Spacing to Obstacle Height	Ratio of Obstacle Spacing to Hydraulic Diameter	Active Electrode Area (cm^2)
0	-	-	24.2 cm^2
3	166.67	27.6	24.1 cm^2
15	41.67	6.9	23.6 cm^2
31	20.73	3.4	23.0 cm^2
49	13.39	2.2	22.3 cm^2

Table II. Comparison of Limiting Current and Interferometry Results at Re=756.

Number of Obstacles	Average boundary layer thickness from limiting current tech. (cm)	Average boundary layer thickness from interferometric tech. (cm)
unobstructed	0.025	0.022
3	0.006	0.011
15	0.004	0.006

FIGURE CAPTIONS

Fig. 1. Side view of flow channel showing entry section spacers (A,B), electrodes (C,D), an attached square obstacle (E), a detached round obstacle (F), and the location of the pressure taps (G). Flow is from left to right. Size and location of obstacles E and F not drawn to scale.

Fig. 2. Schematic side view of interferometer showing a cross-section of the flow cell.

A	Dual-beam He-Ne laser
B	Mirrors
C	Beam expanders
D	Flow cell cross-section
E	Objective lens
F	Reference lens
G	Beam uniter
J	Camera film plane

Fig. 3. Interferograms of mass transfer boundary layers near a square (0.76 x 0.76 mm) attached obstacle and downstream from it. Re=375, i=3 mA/cm^2. (a) upstream location, (b) immediate downstream location, (c) 5 mm downstream, (d) 22 mm downstream from

obstacle, where the boundary layer thickness is re-established to the value immediately upstream from the obstacle.

Fig. 4. Interferometrically- determined reduction of boundary layer thickness by a triangular obstacle located 16 cm from the leading edge (arrow)). Thickness in unobstructed cell shown for comparison.

Fig. 5. Comparison of the effect of obstacle shape on the downstream mass transfer boundary layer. All obstacles are attached to the electrode 16 cm from the leading edge. (A) round, (B) square, and (C) triangular cross-section. Re = 756; $i = 3\ mA/cm^2$.

Fig. 6. Comparison of the effect of obstacle location on the downstream mass transfer boundary layer. Square obstacles are detached (A) 2.29 mm, (B) 1.52 mm, and (C) 0.76 mm from the electrode surface. Re = 756; $i = 3\ mA/cm^2$.

Fig. 7. Current response to a potential step at time zero. The magnitude of the step was in the limiting current plateau region. Effect of increasing Reynolds number (Re) is shown for the unobstructed channel.

Fig. 8. Limiting current as a function of flow rate. Note that increasing the number of obstacles from 31 to 49 does not increase the limiting current.

Fig. 9. Dimensionless plot of mass transfer rates. Note that the analytic solution (Rousar et al., 1971) for the

unobstructed duct is only valid for the laminar regime.

Fig. 10. Pressure drop as a function of flow rate and number of obstacles. Linear relationship for laminar flow in the unobstructed duct indicated by solid line.

Fig. 11. Dependence of measured friction factors on Reynolds number. Solid line depicts the analytic solution for the laminar flow regime in a square duct.

Fig. 12. Recirculation zone downstream from a rectangular cross-section rod Re = 116; flow from left to right. Hydrogen bubbles tracing the flow paths were generated upstream.

Fig. 13. Flow visualization using a diluted Merlmaid AA(Mearl Corp., New York) suspension in water. Obstacle spacings 31 on left, 49 on right. A: Re = 257, B: Re = 900, C: Re = 1,509. In Figs. B and C, shorter (10^{-4} sec.) exposures were used.

Fig. 14. Effect of multiple obstacles on the boundary layer thickness. Location of four attached square obstacles indicated by arrows. By adjusting the distance between obstacles, the average boundary layer thickness can be controlled to avoid increase in the downstream direction. Re = 756; i = 3 mA/cm^2.

Fig. 15. Specific power (W/m^2) requirement for mass transfer coefficient k(cm/sec) obtained with 0, 3, 15, 31 and 49 square obstacles of 0.76 mm height.

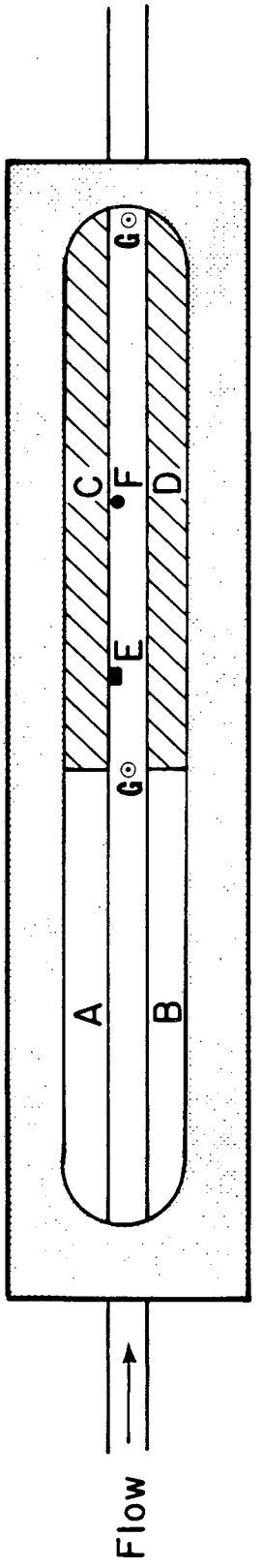

XBL 793-881-B

Fig. 1

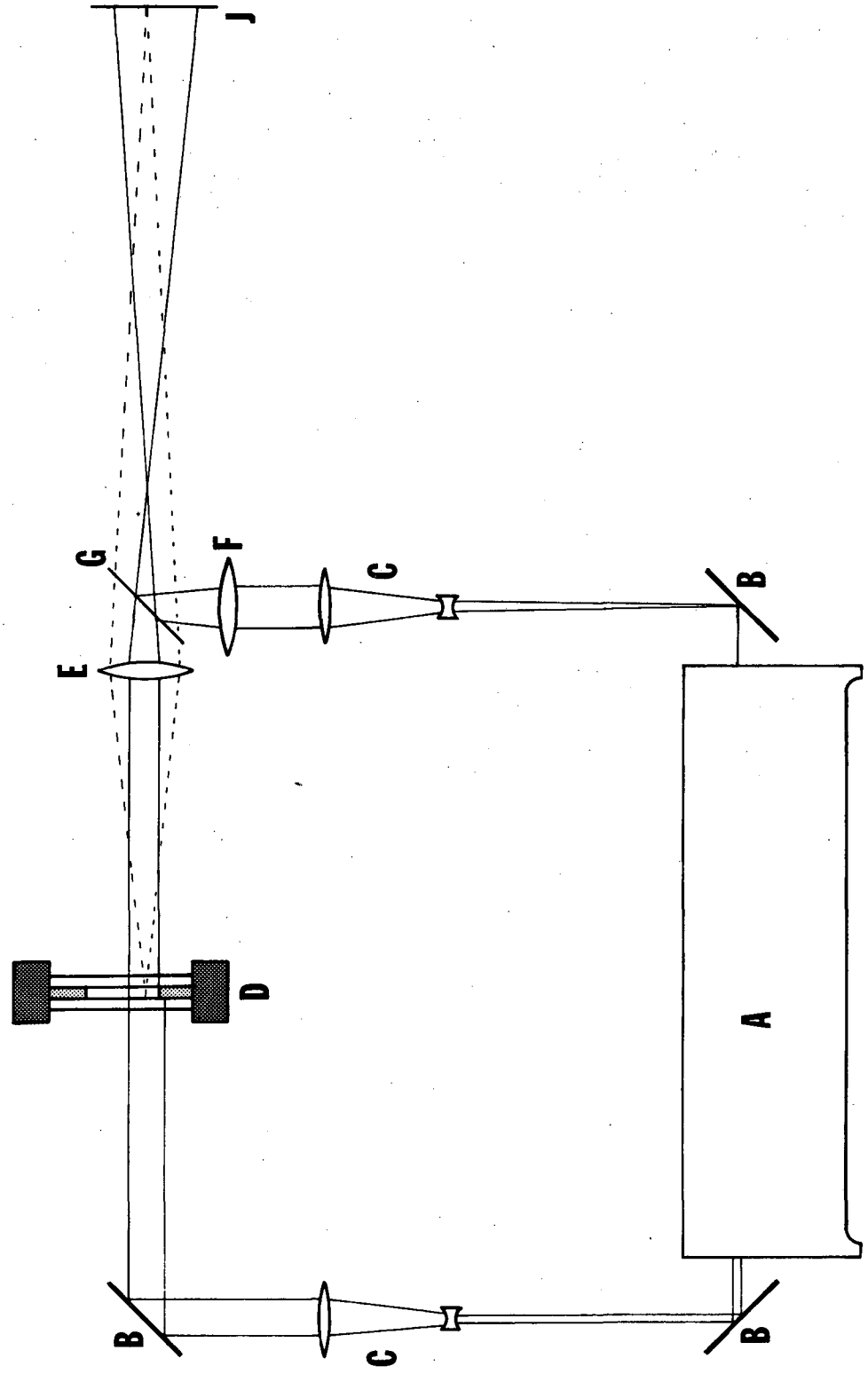

XBL 8412-5417

Fig. 2

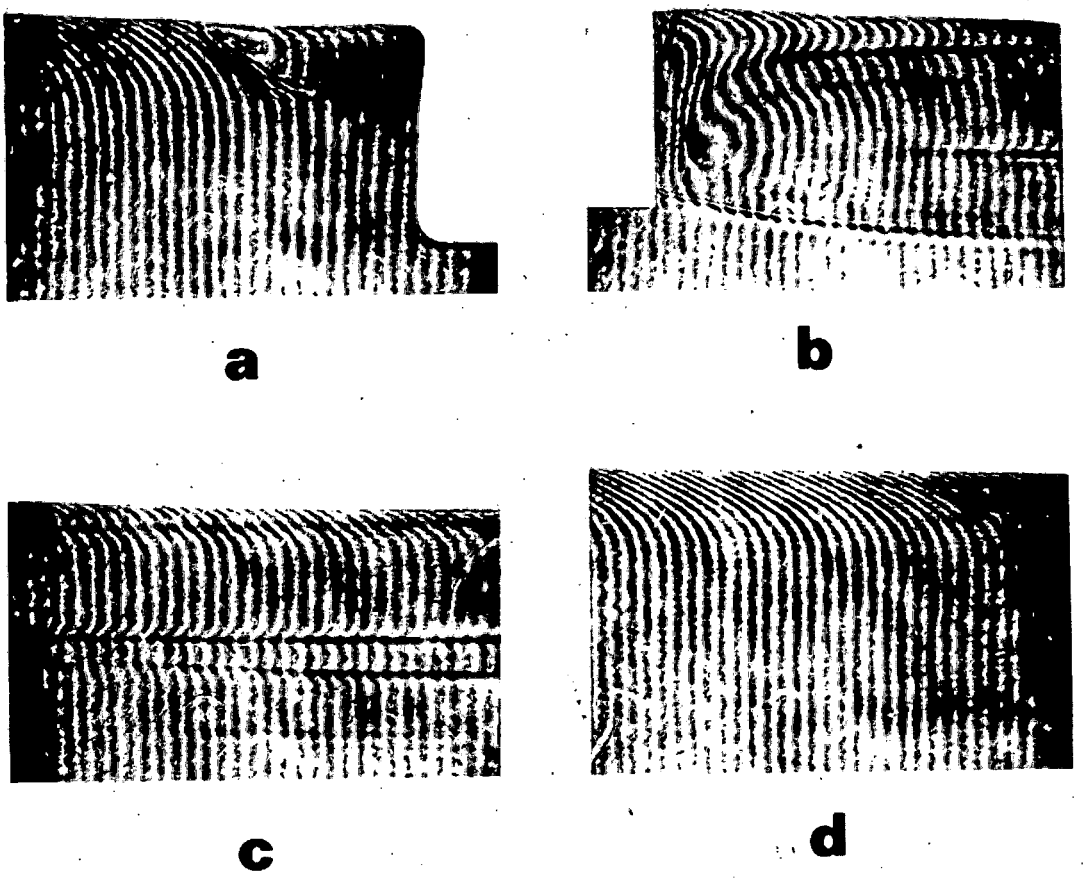

XBB793-4082

Fig. 3

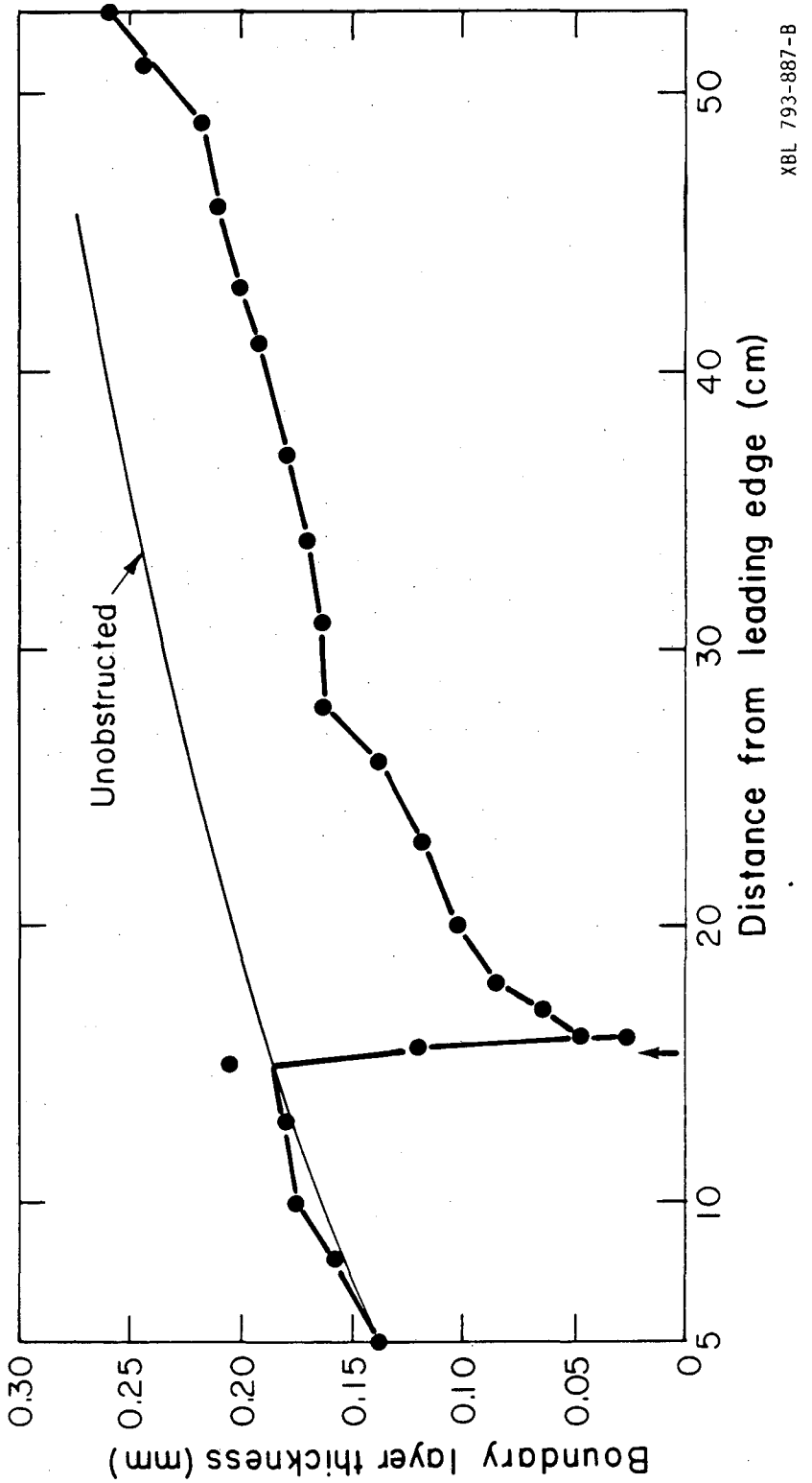
Boundary layer thickness (mm)
0.30
0.25
0.20
0.15
0.10
0.05
0
5
10
20
30
40
50
Distance from leading edge (cm)
Unobstructed
XBL 793-887-B

Fig. 4

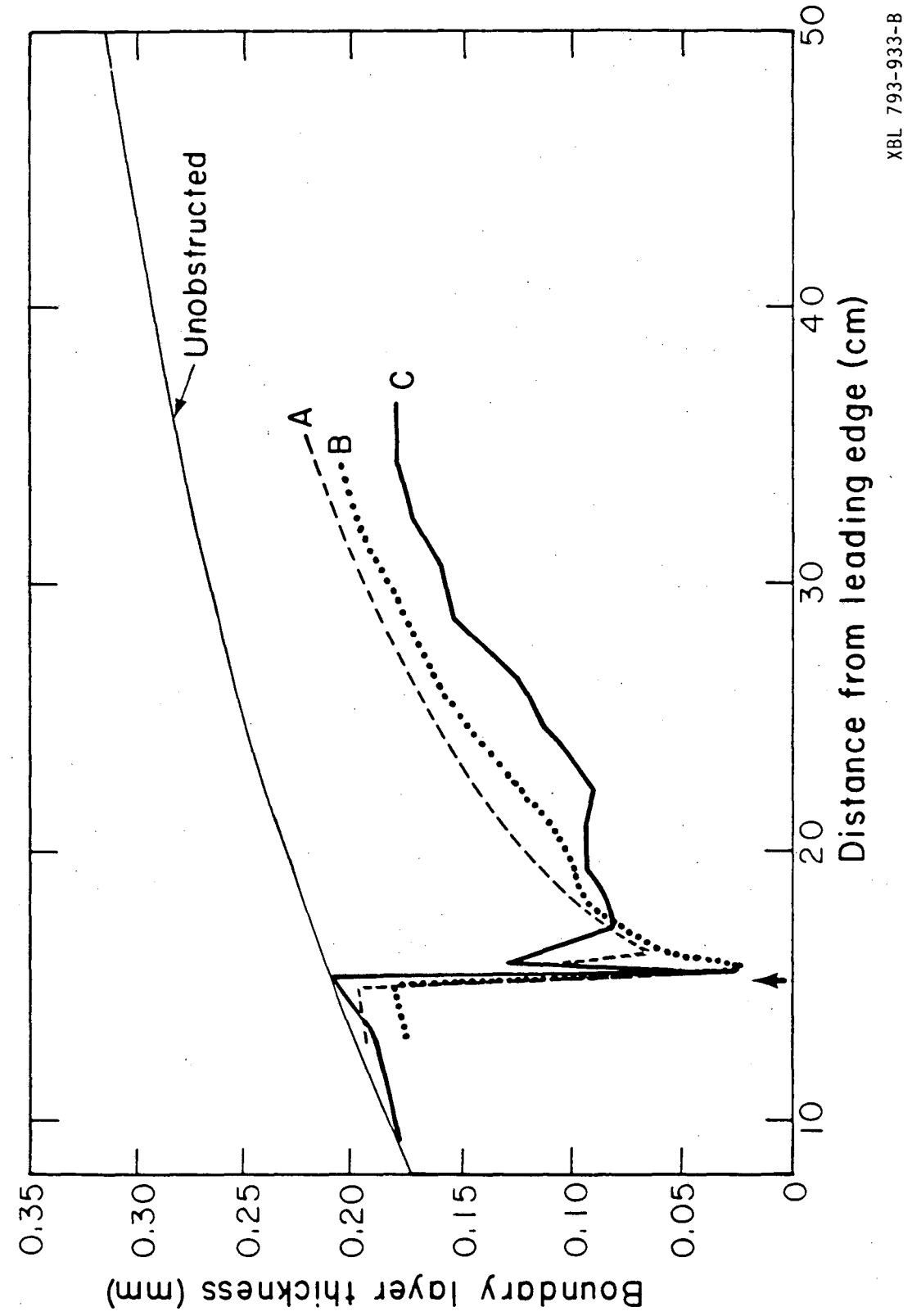

XBL 793-933-B

Fig. 5

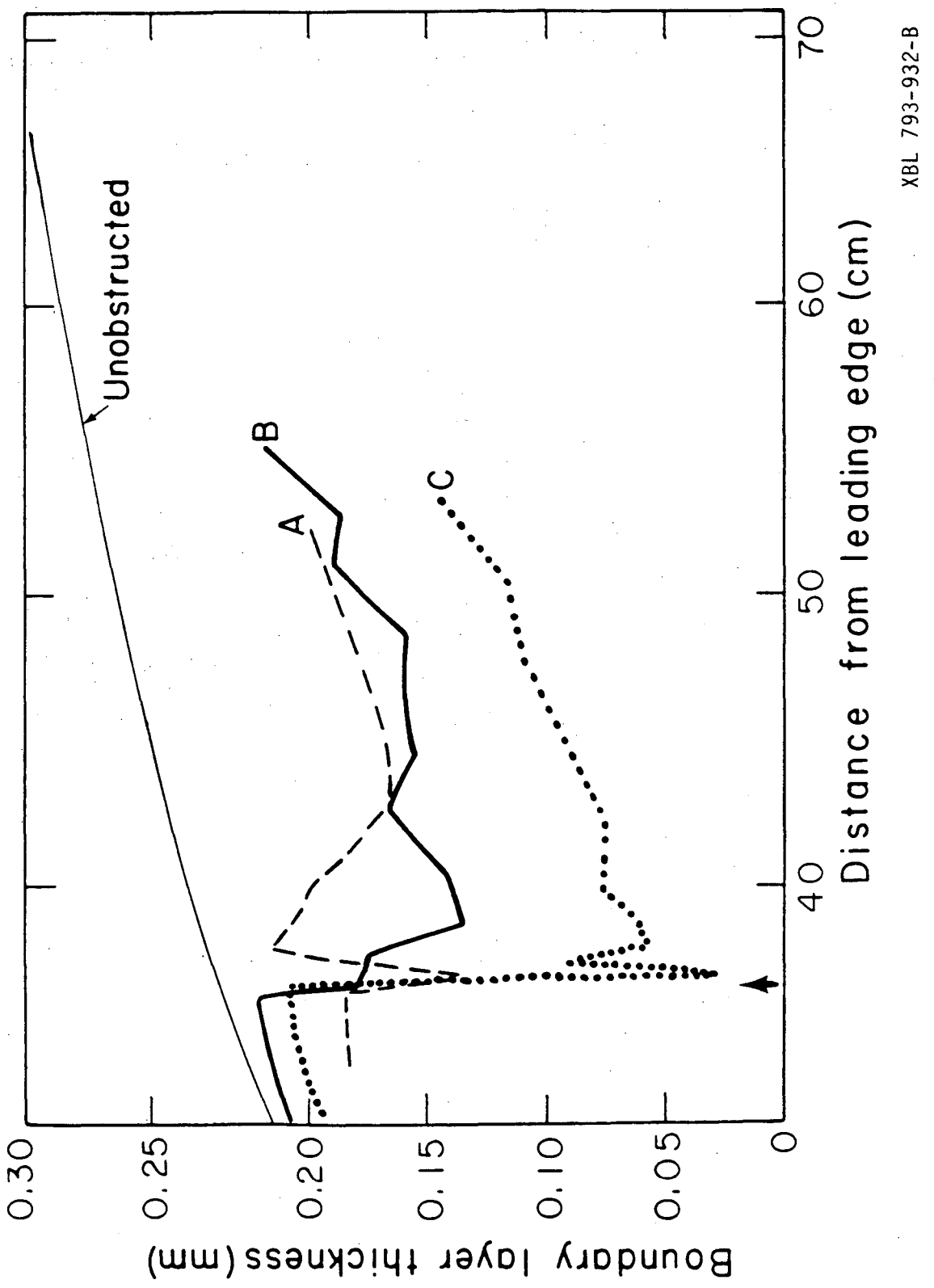

XBL 793-932-B

Fig. 6

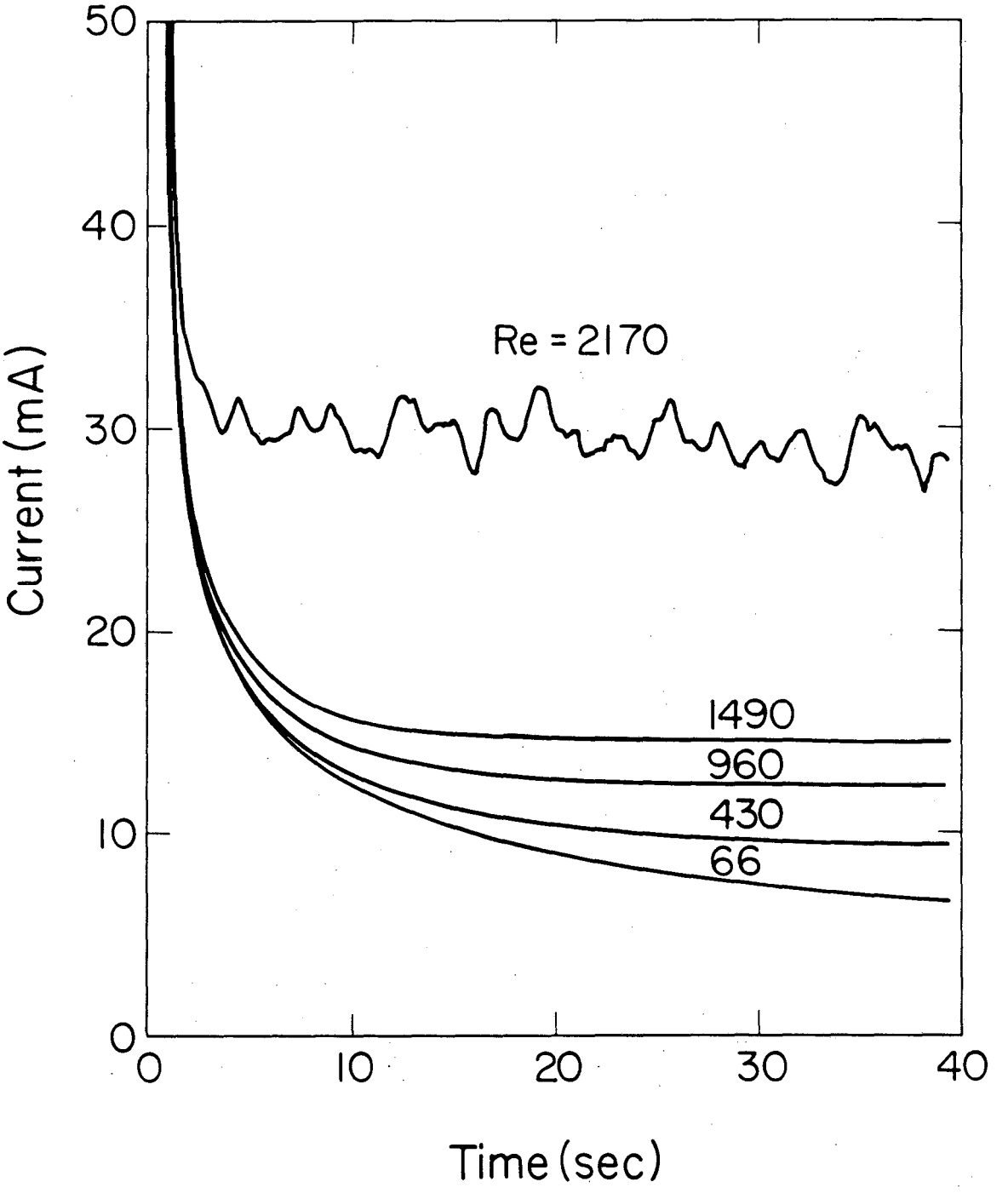
50
40
30
20
10
0
0
10
20
30
40
Current (mA)
Time (sec)
Re = 2170
1490
960
430
66
XBL 835-2633

Fig. 7

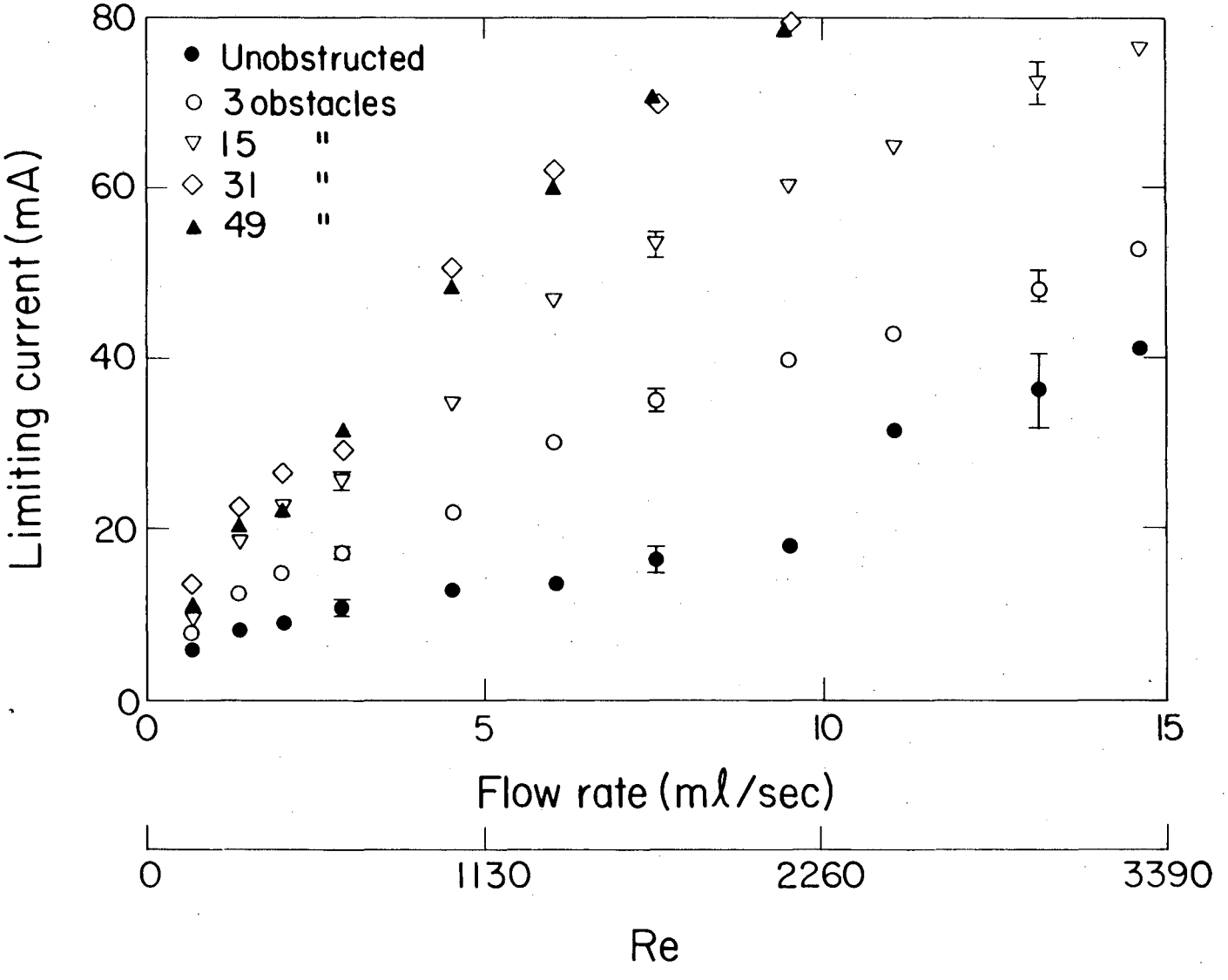
Limiting current (mA)
80
60
40
20
0
Unobstructed
3 obstacles
15 "
31 "
49 "
0
5
10
15
Flow rate (mℓ/sec)
0
1130
2260
3390
Re
XBL 837-2818

Fig. 8

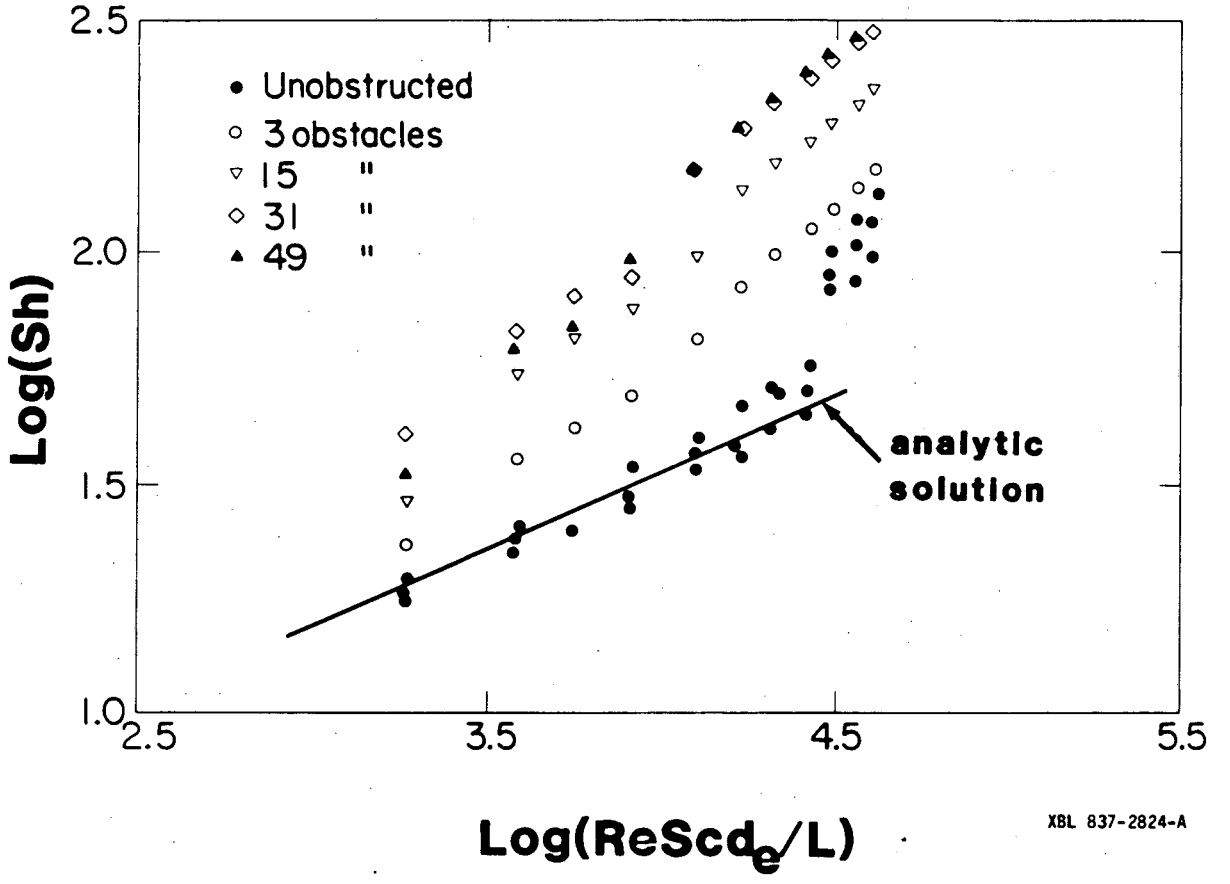
2.5
2.0
1.5
1.0
2.5
3.5
4.5
5.5
Log(Sh)
Log(ReScd$_e$/L)
• Unobstructed
○ 3 obstacles
▽ 15 "
◇ 31 "
▲ 49 "
analytic solution
XBL 837-2824-A

Fig. 9

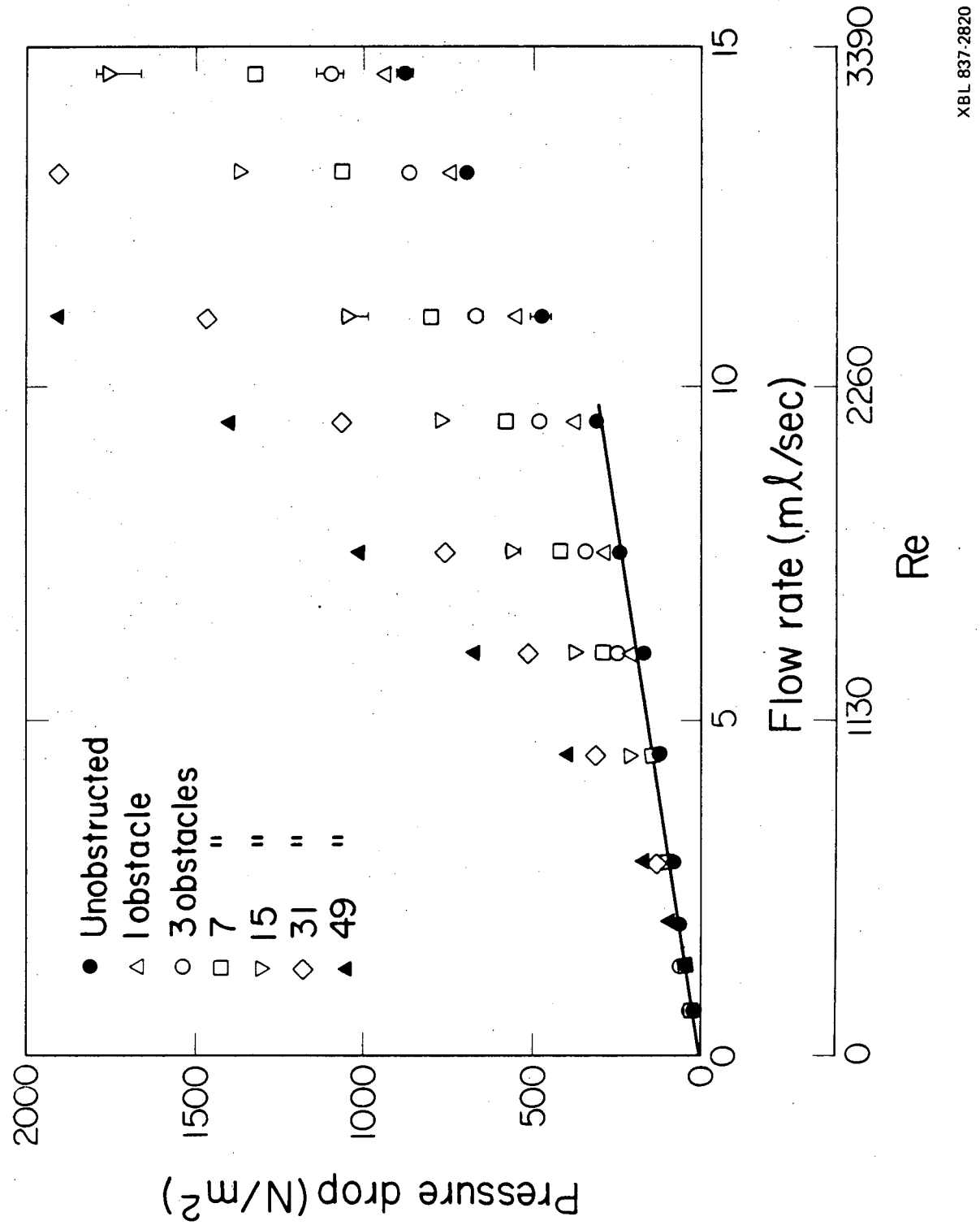
Pressure drop (N/m²)
2000
1500
1000
500
0
0
5
10
15
Flow rate (mℓ/sec)
0
1130
2260
3390
Re
● Unobstructed
△ 1 obstacle
○ 3 obstacles
□ 7 "
▷ 15 "
◇ 31 "
◀ 49 "
XBL 837-2820

Fig. 10

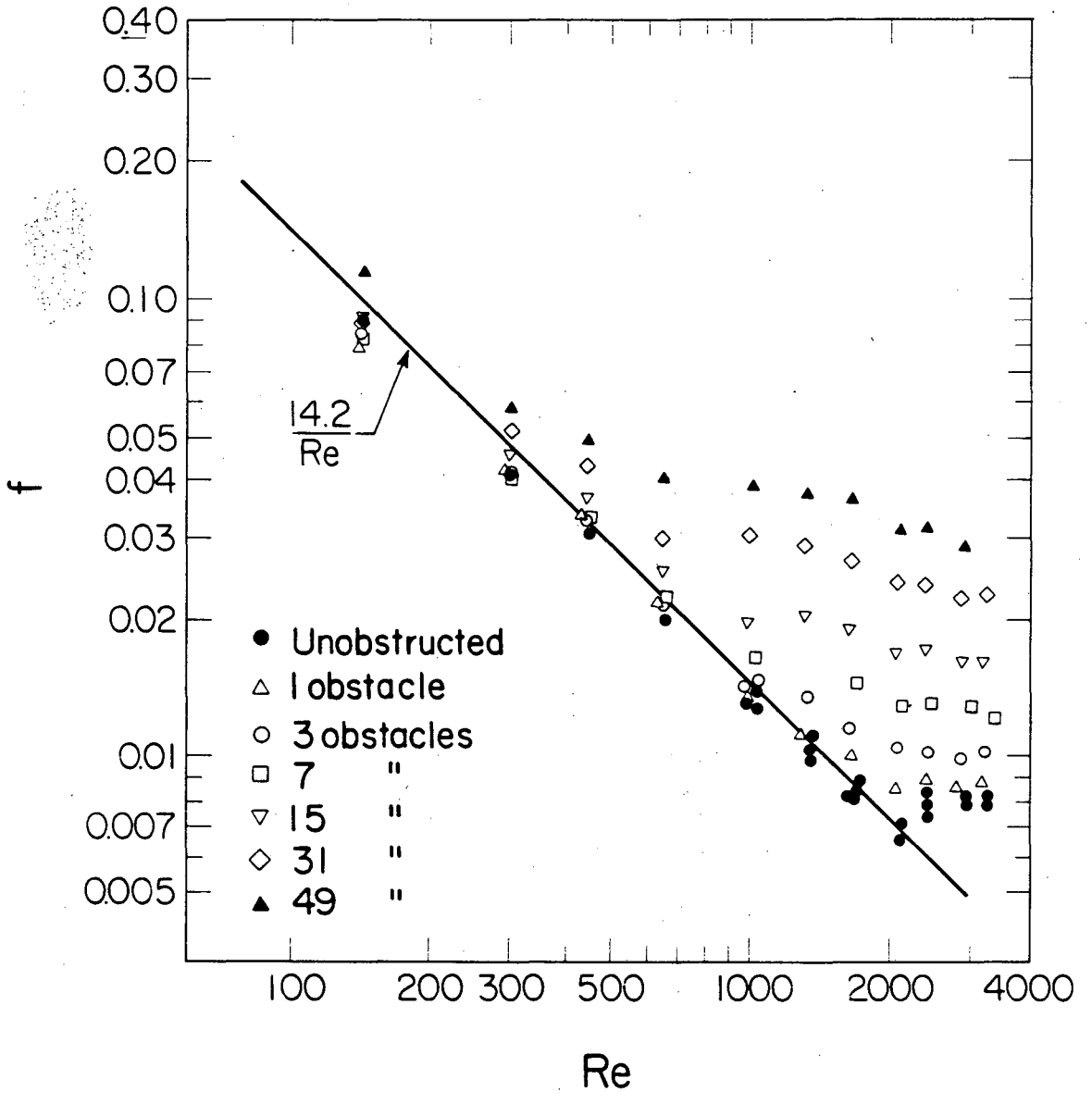
0.40
0.30
0.20
0.10
0.07
0.05
0.04
0.03
0.02
0.01
0.007
0.005
f
14.2/Re
Unobstructed
1 obstacle
3 obstacles
7 "
15 "
31 "
49 "
100
200
300
500
1000
2000
4000
Re
XBL 837-2825

Fig. 11

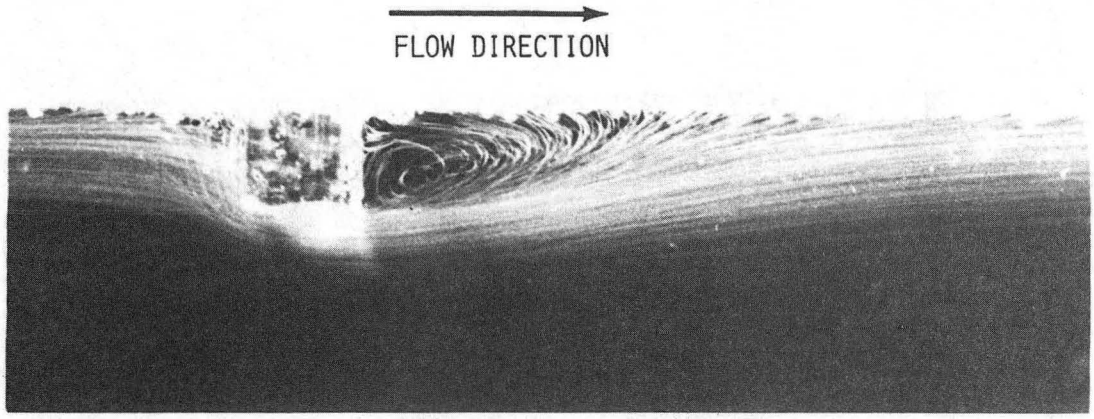

XBB832 1711A

Fig. 12

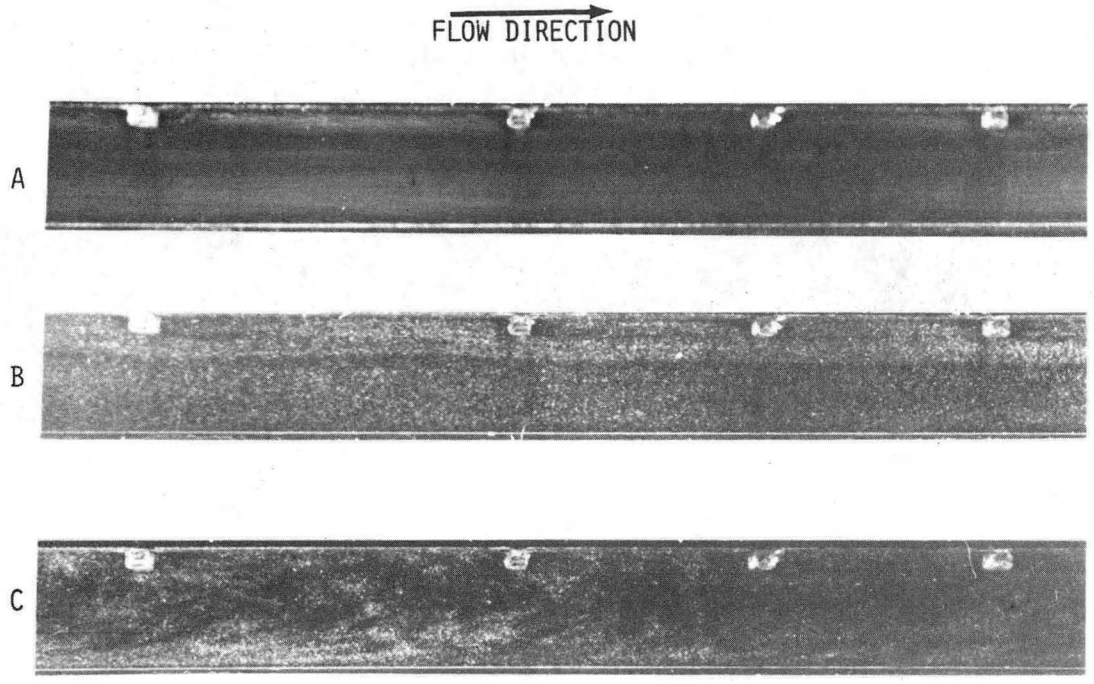

XBB836 5771 A

Fig. 13

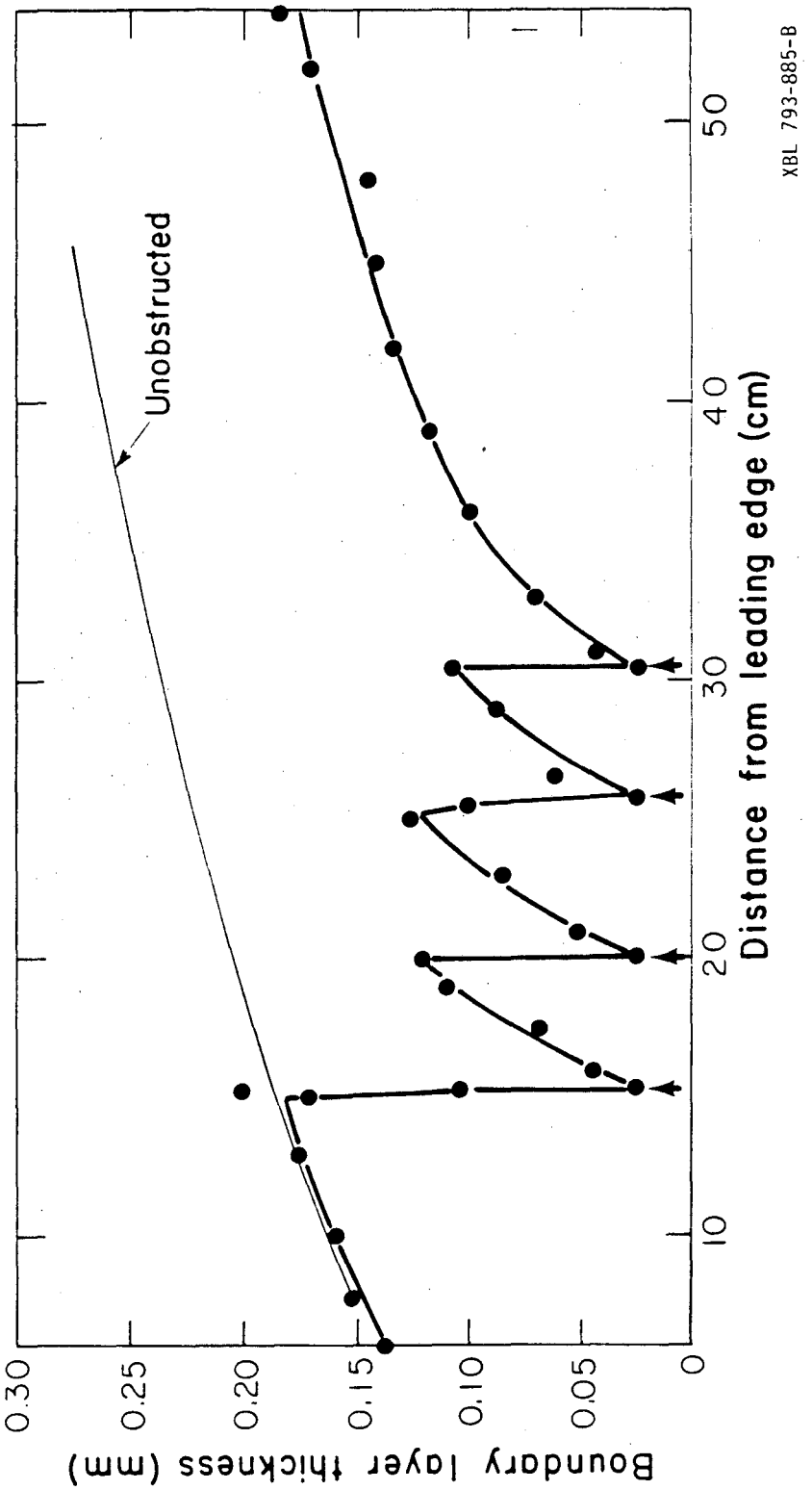
Boundary layer thickness (mm)
0.30
0.25
0.20
0.15
0.10
0.05
0
10
20
30
40
50
Distance from leading edge (cm)
Unobstructed
XBL 793-885-B

Fig. 14

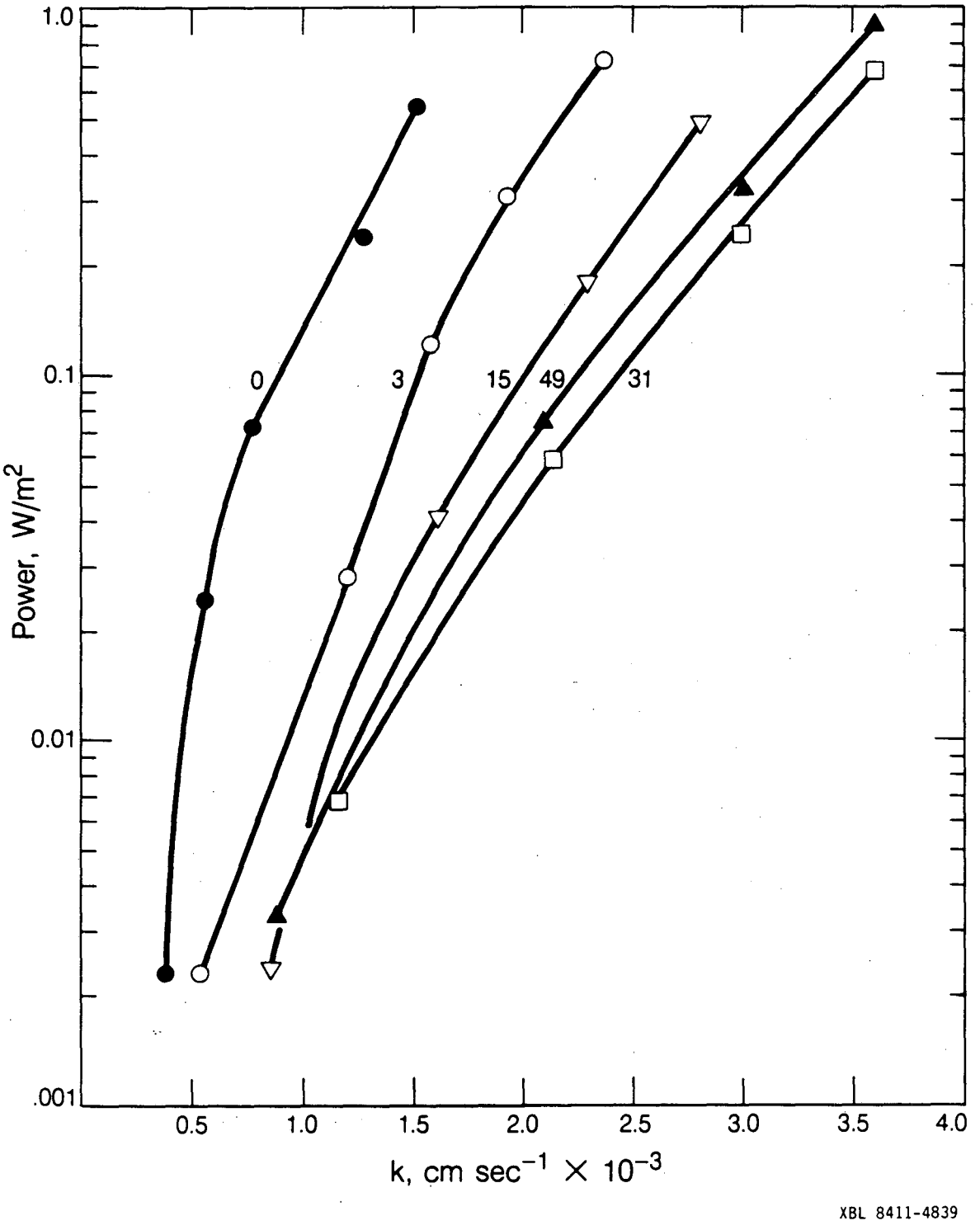
1.0
0.1
0.01
.001
Power, W/m²
0
3
15
49
31
0.5
1.0
1.5
2.0
2.5
3.0
3.5
4.0
k, cm sec⁻¹ × 10⁻³
XBL 8411-4839

Fig. 15

TECHNICAL INFORMATION DEPARTMENT
LAWRENCE BERKELEY LABORATORY
UNIVERSITY OF CALIFORNIA
BERKELEY, CALIFORNIA 94720